Published in Physical Review Letters 42, issue 10, 5984-5989, 1990
which should be used for any reference to this work

M and *N* core excitations in zirconium

F. Vanini, M. Erbudak, P. Aebi,* and G. Kostorz
Institut für Angewandte Physik, Eidgenössische Technische Hochschule Zürich, CH-8093 Zürich, Switzerland

The structures in the electron-energy-loss spectra for the long-lived 3*p*, 3*d*, and 4*s* core excitations in clean zirconium are accounted for by the unoccupied density of states. Transitions to final states with different angular momenta are observed. The short-lived 4*p* excitations can only be understood in terms of an atomic theory given by Fano that treats excitation and relaxation processes simultaneously. It is concluded that the spatial overlap of the atomic wave function of different initial states with those of the 4*d*-projected final states are responsible for these observations.

INTRODUCTION

A primary electron interacting with an atom can lose energy by exciting a core electron of the target. The final-state energy is shared by the two electrons subject to the conservation of energy and momentum. The lifetime of the core-hole state thus created is of general interest. If it is long compared to the excitation process, the inner-shell ionization and the Auger decay process may be separately treated. Then, a two-step model is applied dealing independently with the ionization and subsequent Auger transition.[1] If, on the other hand, the core-hole state has a short life time due to fast decay channels, i.e., super-Coster-Kronig (sCK) processes, then the two-step model is no longer justified; the primary ionization and the "subsequent" decay must be handled simultaneously.[2] In the case of a long-lived core-hole state, if one of the electrons is left just above the Fermi level, E_F, the excitation spectrum is expected to be determined by the partial density of empty states weighted by the matrix elements describing the transition. The subsequent Auger transition involving the valence band then has a spectral shape which can be derived from the density of occupied states left behind with two more or less interacting holes.

A marked deviation from this behavior was observed for the excitations of 3*p* and 4*p* electrons in 3*d* and 4*d* transition metals, respectively.[3–5] For these short-lived excitations the two-step model breaks down. Further, the large Coulomb interaction between the *np* core hole and the *nd* excited electrons leads to a localization of these transitions and, therefore, a description of the excitation spectra in terms of independent electrons fails.

In a previous communication[6] the broad features pertaining to the 4*p*-excitation spectra of zirconium measured in electron-energy-loss spectroscopy have been accounted for using an atomic theory. The measured spectra were well reproduced by considering the excitation and relaxation processes simultaneously and assuming that the atomic final-state multiplets were broadened by an asymmetric distribution obtained from a theory developed by Fano.[7]

In the present work a more accurate calculation of the 4*p*-4*d* transitions were performed taking into account not only dipole but also monopole and quadrupole transitions and considering the interaction between final-state multiplets which were previously neglected. In the experiment, as the primary energy is lowered the smallest possible momentum transfer in the scattering process is shifted to higher values; consequently, dipole-forbidden transitions become relevant.

Also presented are analogous data obtained at the 4*s*, 3*p*, and 3*d* edges for which the lifetime of the core state is relatively long. Hence, they can be explained by the transitions to final states above E_F, mainly composed of unoccupied 4*d* states.

In the following sections, first the Fano theory for interacting discrete and continuum states is recapitulated since this formalism makes possible a coherent treatment of the excitation and relaxation events, and the approximations made are discussed. Subsequently, experimental details are outlined, and the next section is devoted to the results and their discussion. The final section contains the conclusions.

THEORY

The theory of Fano[7] considers an atomic system with a set of discrete states $|\phi_1\rangle \ldots |\phi_n\rangle$ which experience configuration interaction with a set of states $|\psi_{E'}\rangle$ belonging to a continuous spectrum. The portion of the energy matrix corresponding to these states is given by

$$\langle \phi_n | \underline{H} | \phi_m \rangle = E_n \delta_{nm} \ , \tag{1}$$

$$\langle \psi_{E'} | \underline{H} | \phi_n \rangle = V_{E'n} \ , \tag{2}$$

$$\langle \psi_{E''} | \underline{H} | \psi_{E'} \rangle = E' \delta(E'' - E') \ . \tag{3}$$

The δ factors in (1) and (3) imply that the submatrix belonging to the subsets of states $|\phi_n\rangle$ and $|\psi_{E'}\rangle$ has previously been diagonalized. The wave functions of the discrete states are dimensionless, while those of the continuum are normalized per unit energy and have dimension of one over the square root of energy. The discrete energy levels E_n lie within the continuous range of values E'. Each value E within the range of E' is an eigenvalue of the matrix (1,2,3). The diagonalization of this matrix leads to the determination of the eigenvector:

$$|\Psi_E\rangle = \sum_n a_n |\phi_n\rangle + \int dE' b_{E'} |\psi_{E'}\rangle \ , \tag{4}$$

where a_n and $b_{E'}$ are functions of E and are determined as solutions of the system of equations pertaining to the matrix (1,2,3). Carrying out the calculation, the transition matrix element of the transition operator $\underline{T}$ between the initial state $|i\rangle$ and the energy eigenstate $|\Psi_E\rangle$ can be written as:[7]

$$\langle \Psi_E|\underline{T}|i\rangle = \left[\sum_n \frac{\tan\Delta_n}{\pi V_{nE}}\langle \Phi_n|\underline{T}|i\rangle - \langle \psi_E|\underline{T}|i\rangle\right]\cos\Delta \ , \tag{5}$$

where

$$|\Phi_n\rangle = |\phi_n\rangle + \mathrm{P}\int dE' \frac{V_{E'n}}{E-E'}|\psi_{E'}\rangle \ , \tag{6}$$

$$\tan\Delta = -\sum_n \frac{\pi|V_{En}|^2}{E-E_n} = \sum_n \tan\Delta_n \ , \tag{7}$$

and P indicates the principal part of the integral.

In the present work calculations of the $4p$-$4d$ transitions in Zr were carried out using Eq. (5) with the following approximations. (1) the second term in Eq. (6) was neglected as it was assumed to be small. (2) the transition matrix element to the continuum states was taken to be constant, $\langle \psi_{E'}|\underline{T}|i\rangle = \beta$. (3) the matrix elements V_{nE} representing the amount of mixing of the discrete states and the continuum were taken to be proportional to the matrix elements of the transition to the discrete states, i.e.,

$$V_{nE} = V_{En} = \alpha\langle \phi_n|\underline{T}|i\rangle \ ,$$

supposing that the main contribution is the normalization constant of the wave function $|\phi_n\rangle$.

Introducing these approximations Eq. (5) becomes

$$\langle \Psi_E|\underline{T}|i\rangle = \left[\left[\sum_n \frac{\pi\alpha^2|\langle \phi_n|\underline{T}|i\rangle|^2}{E-E_n}\right]^2 + 1\right]^{-1/2} \times \left[\sum_n \frac{\alpha}{E-E_n}\langle \phi_n|\underline{T}|i\rangle^2 + \beta\right] . \tag{8}$$

In Zr the discrete states $|\phi_n\rangle$ were represented by the $4p^6 4d^2 \rightarrow 4p^5 4d^3$ final-state multiplets which decay by a sCK transition to $4p^6 4d^1$ under emission of an electron. This state belongs to a continuum giving rise to the configuration interaction between the discrete states and the continuum. The energies and the wave functions of the initial and the final states were calculated using an atomic multiconfigurational Dirac-Fock (MCDF) program[8] using a jj coupling scheme. The total angular momentum of the initial state was chosen according to Hund's rules. The package was adapted to allow the diagonalization of the energy matrix for 200 multiplet components. The matrix elements $\langle \phi_n|\underline{T}|i\rangle$ were calculated using the subroutine MCT of the MCDF program. This routine computes the coefficients $d^k_{ab}(T,T')$ of the matrix element of the single-particle tensor operator $\langle a\|\mathrm{f}^{(k)}\|b\rangle$:[9]

$$\langle TM|\mathrm{F}^{(k)}_q|T'M'\rangle = \langle J'kJ,M|J'M',kq\rangle \times \langle T\|\mathrm{F}^{(k)}\|T'\rangle = \langle J'kJ,M|J'M',kq\rangle \times \sum_{a\le b} d^k_{ab}(T,T')\langle a\|\mathrm{f}^{(k)}\|b\rangle \ , \tag{9}$$

where $\mathrm{F}^{(k)}_q = \sum_i \mathrm{f}^{(k)}_q(i)$ is an n-electron irreducible tensor operator of rank k, $|TM\rangle$ and $|T'M'\rangle$ are configuration state functions obtained by coupling of n electrons. For the dipole operator $\underline{D}$ one has:[10]

$$\langle a\|\underline{D}\|b\rangle = (-1)^{j_b+1/2}\begin{pmatrix} j_b & 1 & j_a \\ -\frac{1}{2} & 0 & \frac{1}{2}\end{pmatrix} \times\sqrt{2j_b+1}\int r(P_aP_b + Q_aQ_b)dr \tag{10}$$

with j_a and j_b the total angular momentum, P_a, Q_a and P_b, Q_b the large and small components of the relativistic wave function of $|a\rangle$ and $|b\rangle$, respectively, and the term in parenthesis a Wigner $3j$ symbol.

The parameters α and β in Eq. (8) were adjusted to give the best fit with the experimental data. Because of the great oscillations occurring between the different resonances, i.e., when $E = E_n$, a smoothing of the calculated spectrum was achieved by broadening the calculated curve by a Gaussian function with variable width.

In the case of monopole and quadrupole transitions the matrix elements were calculated neglecting the third term in Eq. (9). This approximation resulted to be feasible from the comparison of dipole matrix elements computed with and without Eq. (10).

EXPERIMENTAL

Electron-energy-loss spectroscopy (EELS) measurements were performed in an ultra-high-vacuum system with a total pressure of 10^{-8} Pa. An electron gun produced a monoenergetic electron beam with a current of 5 μA. The energy of the backscattered electrons was analyzed using a Riber Mac 2 energy analyzer. In this type of analyzer the energy analysis of the electrons focused by an input lens is obtained by combining a two-grid retarding stage with a dispersive energy filter. The energy resolution is constant over the whole energy range and was chosen between 0.40 and 0.75 eV depending on the available signal intensity. The electron current was detected using a channel electron multiplier operating in analog mode. The output signal was fed, after amplification 10^8 times, to a voltage-to-frequency converter and to a counter. Data collection and sweeping the energy analyzer were controlled by a PDP 11 microcomputer.

Clean Zr surfaces were prepared by Ar^+ sputtering, provided by a hybrid gun,[11] until carbon and oxygen Auger signals were below the limit of detectability. The measurements were performed under continuous Ar^+ bombardment in order to prevent the contamination of the reactive surface.

RESULTS AND DISCUSSION

In an independent-electron approximation and provided that the two-step model applies, the EELS spectra of np edges ($n=2,3,4$) of Zr should show the structures of the density-of-states (DOS) above E_F, in particular the $4d$ partial DOS considering that the dipole transitions provide the dominant part of the excitations. The DOS of metallic Zr calculated and measured with Bremsstrahlung Isochromat Spectroscopy (BIS) extends over a width of ~ 7 eV with two main structures appearing 1 and 5 eV above E_F.[12,13] Since the major contribution to the total unoccupied DOS near E_F is thought to originate from the $4d$ states, it is expected that the np edges of Zr exhibit structures dictated by those of the d states. This is confirmed by calculations of the L_3 x-ray-absorption edge by Müller *et al.*[14] They showed that the expected shape of the $2p_{3/2}$ absorption spectrum for Zr should exhibit a width of about 7 eV and be composed of two ill-separated peaks.

The binding energy of Zr $2p$ electrons exceeds 2200 eV. In order to obtain acceptable signal intensities in EELS, one should excite the $2p$ levels with electrons of energies above 3000 eV. This was not possible under the present experimental conditions. On the other hand, the $3p_{3/2}$ and $3p_{1/2}$ electrons, with binding energies of 329.9 and 345.5 eV, respectively,[15] are well suited for such an analysis. Figure 1 (top) illustrates the $3p$-$4d$ transitions of Zr measured in EELS with primary energies of 650 and 2300 eV. The two similar peaks appearing at 331.3 and 344.5 eV represent the excitations of the $3p_{3/2}$ and $3p_{1/2}$ electrons, respectively. For the lower primary energy the dipole approximation loses its validity, allowing multipole transitions to occur with increasing probability. However, the two curves measured with different primary energies show no significant differences. The $3p$-$4d$ transitions which are dominant at a primary energy of 2300 eV still remain strong at lower energies because of the large d DOS compared to the contribution of the other angular momentum components near E_F.

Multiple-scattering cluster calculations were also performed for the different angular-momentum components of the unoccupied density of states in zirconium, using an extended version of the ICXANES (Ref. 16) program. The result for the unoccupied part of the d band is also shown in Fig. 1. The bottom part contains the "raw" data; the smooth curve is obtained after a broadening by a Gaussian function. A value of 2 eV was chosen as full width at half maximum for the best fit with the measurements. Since the resolution of the spectrometer was 0.7 eV, the broadening of these transitions is mainly due to the limited lifetime of the $3p$ hole. In fact, in x-ray photoemission spectroscopy (XPS) spectra the width of the $3p$ lines is about 5 eV.[17] For this reason all the structures appearing in the calculated d DOS and measured in BIS (Refs. 12 and 13) are not discernible in this case.

The calculated d DOS as presented in Fig. 1, accounts well for the shape of the $3p$-$4d$ transitions in Zr. It was communicated earlier[6] that the $4p$-$4d$ excitations, on the contrary, behave unexpectedly. This is evident from Fig. 2 (upper curve) where the $4p$-$4d$ transitions are shown, measured with a primary energy of 2000 eV. The broad loss feature between 26 and 46 eV is assigned to the $4p$-$4d$ excitation spectrum. The width of this emission exceeds that of the $3p$-$4d$ transitions by a factor of about 3. In this case, the $4p$ hole decays via the fast $4p4d4d$ sCK transition and the two-step model is not applicable any

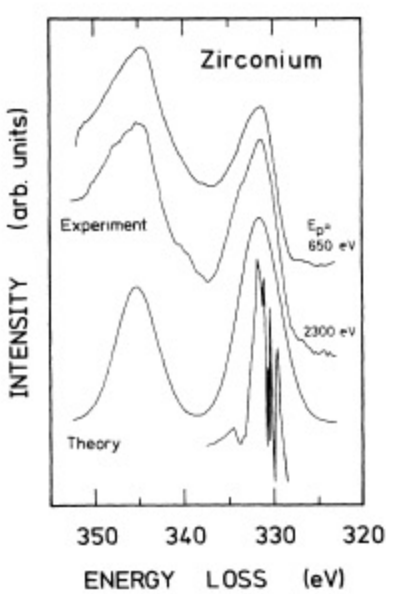

FIG. 1. EELS spectra of Zr obtained with a primary energy of 650 and 2300 eV (top). The calculated spectrum (smooth curve) is obtained by broadening with a Gaussian function the calculated $4d$ partial DOS (bottom).

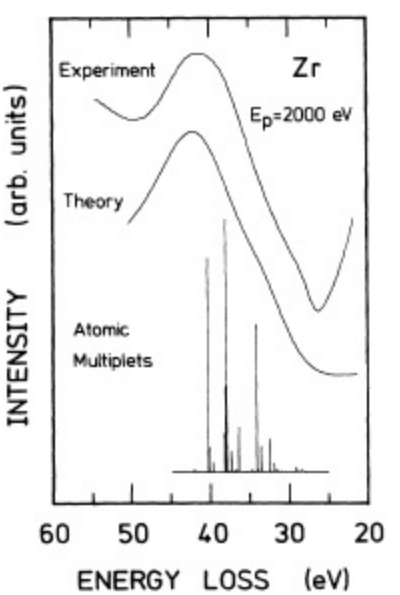

FIG. 2. EELS spectrum (upper curve) and calculated curve using the final-state multiplets of the $4p^6 4d^2 \rightarrow 4p^5 4d^3$ transition broadened by Fano resonances (lower curve) of Zr. The vertical bars show the energy and dipole oscillator strength of the multiplets for a Zr atom.

more. Further, owing to the large Coulomb interaction between the $4p$ hole and the excited $4d$ electrons, the independent-electron description breaks down. Therefore, the $4p$-$4d$ transitions resemble those of an isolated atom, and the structure of the loss spectrum arises from the $4p^6 4d^2 \rightarrow 4p^5 4d^3$ excitation multiplets (Fig. 2, vertical bars), broadened by Fano resonances that take into account the relaxation of the excited state. In the calculations, a $4p^6 4d^2 5s^2$ configuration was taken for the initial state according to the occupation of the orbitals for a Zr atom, and a total angular momentum $J_i = 2$ was assumed for the ground state following Hund's rule. For the final state the total angular momentum J_f was set $J_f = J_i, J_i \pm 1$ in agreement with the dipole selection rules. The matrix elements were obtained from Eqs. (9) and (10). Figure 2 (lower curve) shows the calculated $4p$-$4d$ transitions obtained after broadening the multiplet components by Fano resonances using Eq. (8). The agreement between the measured and the calculated curves is good, supporting the atomic character of the $4p$-$4d$ transitions in Zr and the strength of the Fano theory for treating the dynamics of interacting excitation and relaxation processes.

In order to shed light on the time scale of the relaxation processes via which an np hole decays involving the $4d$ electrons, radial wave functions of the $2p$, $3p$, $4p$, and $4d$ electrons were calculated for a Zr atom. The results are exposed in Fig. 3 as a function of the radial distance given in units of the Bohr radius. While the $2p$ and $3p$ wave functions are mainly limited to distances below 1 a.u. from the nucleus, the main part of the $4p$ and $4d$ wave functions are spread over a width of more than 2 a.u. The pronounced overlap of the $4p$ and $4d$ wave functions favors a strong exchange interaction between the $4p$ hole and the $4d$ electrons. This interaction is responsible for the splitting of the $4d^3$ state in its multiplets since the occupied $4d$ band of Zr is quite narrow in the ground state and an additional electron acts as a strong perturbation. Furthermore, it favors the fast decay of the $4p$ hole via a $4p4d4d$ sCK transition.

The $4p$ excitation spectra of Zr measured in EELS with different primary energies are shown in Fig. 4. A large energy interval is displayed in the figure such that it includes a structure appearing between 52 and 63 eV which

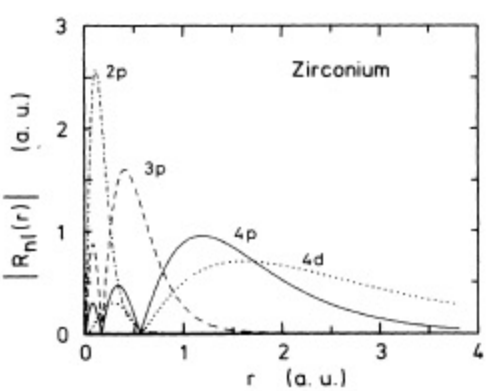

FIG. 3. Radial wave functions of the $2p$ (dash-dotted), $3p$ (dashed), $4p$ (solid) and $4d$ (dotted curve) electrons calculated for a Zr atom.

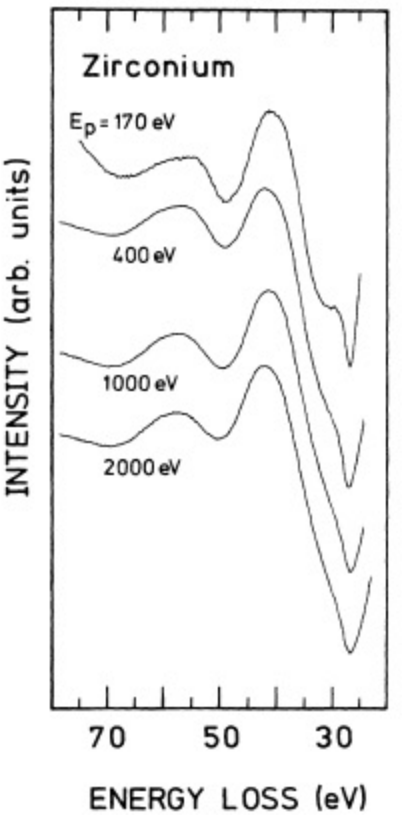

FIG. 4. EELS spectra of Zr taken with different primary electron energies in the energy region of the $4s$ and $4p$ excitations.

is related to the excitations of the $4s$ electrons. The low-energy-loss side of this peak becomes sharper with decreasing primary energy. This can be explained by the decreasing validity of the dipole approximation as the minimum momentum transfer increases while the excitation energy is lowered. Therefore the $4s$-$4d$ transitions occur with greater probability leading to a sharper structure of the low-energy side of the absorption edge since the d DOS is dominant at and near E_F. The $4p$-$4d$ excitations appear between 27 and 47 eV. The curve measured with $E_p = 2000$ eV was compared in Fig. 2 with the Fano broadened final-state multiplets calculated by applying the dipole selection rule. For decreasing primary energy a shoulder appears on the low-energy-loss side of the transition which develops to a distinct peak at 29.4 eV in the spectrum measured with a primary energy $E_p = 170$ eV. The minimum momentum transfer for an energy loss of 30 eV is 0.17 Å^{-1} for $E_p = 2000$ eV and 0.62 Å^{-1} for $E_p = 170$ eV.[18] Since the excitation probability favors transitions with a low momentum transfer,[19] the minimum momentum transfer is of great importance. As this quantity increases markedly for decreasing primary energy between 2000 and 170 eV, the probability of multipole transitions, in particular monopole and quadrupole

transitions, becomes relevant, too. The peak appearing at 29.4 eV can be related to the $4p^6 4d^2 \rightarrow 4p^5 4d^3$ final-state multiplets with a total angular momentum $J_f = J_i \pm 2$, i.e., $J_f = 0,4$.

Figure 5 illustrates the EELS spectrum (upper curve) measured with 170 eV primary energy and the calculated curve using the final-state multiplets of the $4p^6 4d^2 \rightarrow 4p^5 4d^3$ transitions broadened by Fano resonances (lower curve). Here, the vertical bars show the final-state multiplets for a Zr atom with total angular momentum $J_f = J_i$, $J_i \pm 1$, $J_i \pm 2 = 0,1,2,3,4$, i.e., considering dipole, monopole, and quadrupole transitions. The weighting factors of the different transitions were taken as additional fitting parameters. Still, it should be emphasized that neither the energy positions of the multiplets nor those of the calculated curves were adjusted to fit the measured spectra throughout this work. The overall shape of the transitions is well reproduced by the calculation whereas the maxima of the peaks appear shifted by a few eV.

The general agreement of the two curves and even more significantly the possibility to account for the appearance of the peak on the low-energy-loss side of the $4p$-$4d$ excitations by dipole-forbidden transitions, confirms the validity of the atomic picture for these excitations in Zr. In a noninteracting-electron model the growth of the structure at 29.4 eV with decreasing primary energy cannot be explained. Since the $4p$-$4d$ transitions are dipole allowed and the $4d$ DOS has its maximum near E_F and is dominant relative to the other angular momentum components, a structure appearing at lower energies cannot be attributed to monopole and quadrupole transitions. Such a structure can only appear if transitions not allowed by the dipole selection rules into states just above E_F become possible for low primary-electron energies, as it is the case for the $4s$ excitations.

The interplay between different excitation channels as the minimum momentum transfer is varied, occurs also for the $3d$ edge. The EELS spectrum measured with three different primary energies showing the $3d$ excitations of Zr is displayed in Fig. 6. In these three spectra the onset of the edge is situated at ~ 178 eV and a relative peak at ~ 187 eV is present, with a shoulder between them. The loss spectrum consists of the sum of the contributions of both the $3d_{5/2}$ and the $3d_{3/2}$ electrons which have binding energies of 178.8 and 181.0 eV, respectively.[15] In the measured spectra, the two components are not separated. The height of the first steep increase at the beginning of the edge is a measure of the transition probability to states just above E_F. A comparison of this height with the intensity of the peak at 187 eV shows that the transition probability to states near E_F increases with decreasing primary energy, i.e., with increasing intensity of the dipole-forbidden transitions. Therefore, the structure at low-energy loss can be attributed to the $3d$-$4d$ transitions. In the spectrum measured with $E_p = 480$ eV the $3d_{5/2}$ (at ~ 180 eV) and the $3d_{3/2}$ (at ~ 182 eV) transitions are separated while for higher primary energies the $3d_{3/2}$-$4d$ excitations, having a lower intensity, disappear in the larger peak. Accordingly, the shoulder around 182 eV originates from the $3d_{3/2}$ contribution.

The structure at ~ 187 eV can be related to a dipole-allowed excitations into empty f or p states above E_F. In order to investigate this possibility a cluster calculation has been performed which shows that the f DOS for Zr has a maximum at about 35 eV above E_F and the p DOS

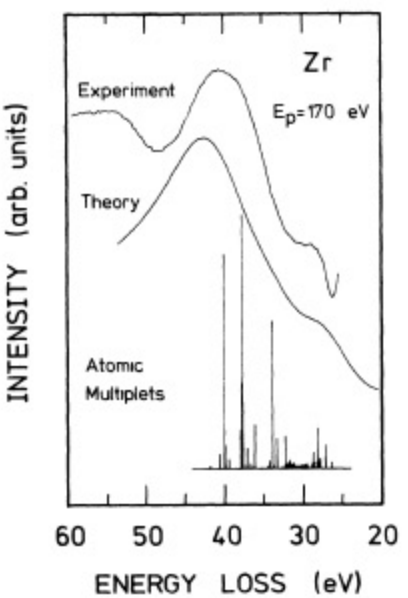

FIG. 5. EELS spectrum (upper curve) and calculated curve using the final-state multiplets of the $4p^6 4d^2 \rightarrow 4p^5 4d^3$ transition broadened by Fano resonances (lower curve) of Zr. The vertical bars show the final-state multiplets for a Zr atom with total angular momentum $J_f = J_i, J_i \pm 1, J_i \pm 2 = 0,1,2,3,4$.

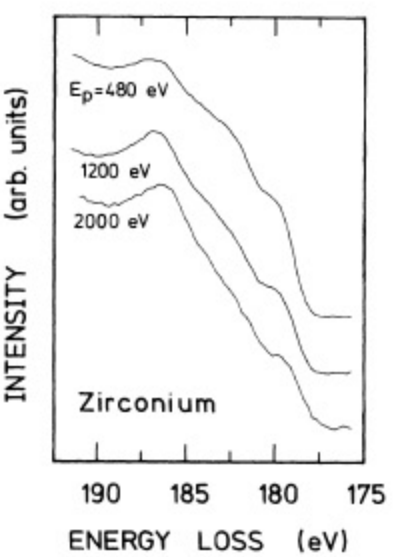

FIG. 6. EELS measured with primary electron energies of 2000, 1200, and 480 eV showing the $3d$ excitations in Zr.

at ~20 eV. Therefore, it is not clear which transition accounts for the peak appearing ~9 eV above E_F. This peak increases markedly upon oxidation of the Zr surface but even this additional information did not bring any further insight into the nature of this structure.

CONCLUSIONS

Excitations of different core electrons were studied for Zr by means of EELS. The 3*p* excitation spectra can be explained by the gross shape of the unoccupied part of the 4*d* DOS. Yet, fine structures appearing in the calculated DOS do not appear in the loss spectra because of the broadening due to the limited lifetime of the core hole. The fact that the spectrum of the 3*p* excitations does not change with different primary energies, i.e., with different minimum momentum transfer, can be related to the dominant 4*d* character of the DOS above E_F, which gives the principal contribution to the spectrum even if quadrupole and monopole transitions become relevant at higher momentum transfer.

The 3*d* edges behave similarly for different primary energies. The low-energy side of the spectrum can be related to the 3*d*-4*d* transitions because this part becomes more pronounced with decreasing primary energy, i.e., with increasing probability of monopole transitions. In this case, an interpretation in terms of the one-electron band structure accounts well for the measured features. An open question is the nature of the marked structure appearing about 9 eV above the edge which cannot be related to any angular momentum component. One should invoke an explanation based on many-body effects and/or a multiple-scattering channel for the excited electrons. An atomic calculation was not performed for this edge since the interaction of the 3*d* hole with the excited 4*d* electrons is not expected to be sufficiently strong to justify the application of an atomic model.

In contrast, the 4*p* edges differ markedly from the expected behavior. The structures related to the 4*p*-4*d* transitions exhibit a width of ~18 eV which is several times the width measured for the 3*p* edges or the width of the empty 4*d* states. Following the work of Dietz *et al.*[3] for the 3*p*-3*d* excitations in the 3*d* transition metals, the shape of the 4*p*-4*d* transitions in Zr can be explained by an atomic model considering the resonant interaction of the excitations to discrete levels and one or several continua and the decay channels. The formalism of such an interaction was given by Fano.[7] The applicability of an atomic model in these solids can be related to the strong interaction between the 4*p* core hole and the excited 4*d* electrons due to the large spatial overlap of the wave functions. The overall agreement between theory and experiment is good and, in particular, it is possible to account for the unexpectedly large width of the measured transition spectra. An additional confirmation of the validity of the theory is given by the appearance of a shoulder at the low-energy-loss side of the 4*p*-4*d* transitions of Zr when the primary energy is low. This shoulder can be explained by final-state-multiplet components that can be excited by quadrupole or monopole transitions which become important for high momentum transfer, i.e., for low primary energy.

Although the agreement between experiment and atomic calculation is good, the theory remains a crude approximation since solid-state effects have been completely neglected. So far, solid-state theories successfully account for excitation and relaxation processes in the limiting case when they occur on a different time scale, i.e., when they are separable. A solid-state theory which takes into account the fast decay of the excited states and consequently its interaction with other excitation channels with the same final state in a solid (as in the Fano theory for atoms) would bring a better understanding of the nature of the 4*p*-4*d* transitions in Zr and other 4*d* transition metals. Analogous problems in the relaxation spectra, e.g., sCK transitions, await the development of such theories.

ACKNOWLEDGMENTS

The authors thank A. Meier for his able technical help. This work was partly supported by the Schweizerischer Nationalfonds zur Förderung der wissenschaftlichen Forschung.

*Present address: Institute for Materials Research, McMaster University, Hamilton, L8S 4M1, Canada.

[1]D. Chatterji, *The Theory of Auger Transitions* (Academic, New York, 1967).

[2]O. Gunnarsson and K. Schönhammer, Phys. Rev. B **22**, 3710 (1980).

[3]R. E. Dietz, E. G. McRae, Y. Yafet, and C. W. Caldwell, Phys. Rev. Lett. **33**, 1372 (1974).

[4]L. C. Davis and L. A. Feldkamp, Solid State Commun. **19**, 413 (1976).

[5]A. Cornaz, M. Erbudak, P. Aebi, F. Stucki, and F. Vanini, Phys. Rev. B **35**, 3062 (1987).

[6]F. Vanini, M. Erbudak, and P. Aebi, Solid State Commun. **66**, 589 (1988).

[7]U. Fano, Phys. Rev. **124**, 1866 (1961).

[8]I. P. Grant, B. J. McKenzie, P. H. Norrington, D. F. Mayers, and N. C. Pyper, Comput. Phys. Commun. **21**, 207 (1980).

[9]N. C. Pyper, I. P. Grant, and N. Beatham, Comput. Phys. Commun. **15**, 387 (1978).

[10]L. Armstrong, W. R. Fielder, and D. L. Lin, Phys. Rev. A **14**, 1114 (1976).

[11]E. B. Bas, E. Gisler, and F. Stucki, J. Phys. E **17**, 405 (1984).

[12]W. Speier, J. C. Fuggle, R. Zeller, B. Ackermann, K. Szot, F. U. Hillebrecht, and M. Campagna, Phys. Rev. B **30**, 6921 (1984).

[13]H. Merz and K. Ulmer, Z. Phys. **210**, 92 (1968).

[14]J. E. Müller, O. Jepsen, and J. W. Wilkins, Solid State Commun. **42**, 365 (1982).

[15]J. C. Fuggle and N. Mårtensson, J. Electron Spectrosc. Relat. Phenom. **21**, 275 (1980).

[16]D. D. Vvedensky, D. K. Saldin, and J. B. Pendry, Comput. Phys. Commun. **40**, 421 (1986).

[17]C. D. Wagner, W. M. Riggs, L. E. Davis, J. F. Moulder, and G. E. Muilenberg, *Handbook of X-Ray Photoelectron Spectroscopy* (Perkin-Elmer, Eden Prairie, 1979).

[18]A. G. Nassiopoulos and J. Cazaux, Surf. Sci. **149**, 313 (1985).

[19]R. D. Leapman, P. Res, and D. F. Mayers, J. Chem. Phys. **72**, 1232 (1980).